distance r_0. When this expression is used with the crystallographic data for the six Rb–O distances[19] in $Rb^+(18C6)\cdot SCN(8C6),SCN^-$, the Rb–O contribution to σ_{stat} was found to be 0.083 Å.

The value of σ_{vib} cannot be independently calculated because the necessary vibrational data are not available. When the experimental Debye–Waller factor is used, it can be estimated to be 0.043 Å. Similar calculations for $Rb^+(18C6),Br^-\cdot 2H_2O$[20] give 0.091 and 0.041 Å for σ_{stat} and σ_{vib}, respectively.

The reduced EXAFS amplitudes obtained for these complexes are also due to the relatively large distances between the rubidium cation and the nearest shell of oxygen neighbors from the ligand (3.00 Å). This causes a reduction in the amplitude because of the r^{-2} dependence of the EXAFS function (eq 1).

Conclusions

The combined use of XANES and EXAFS has permitted the identification and structural characterization of rubidium-containing alkalides and electrides. The white-line areas provide a means of identifying these new products as pure rubidides, electrides, or mixtures. These XANES studies have been especially valuable in identifying the rubidium-containing species in heteronuclear alkalides such as $Rb^+(18C6),Na^-$, $Cs^+(18C6)_2,Rb^-$, and $K^+(C222),Rb^-$. In other cases, they have shown the presence of mixtures of alkalides such as in $RbK(15C5)_2$ and RbK(18C6). They have also been valuable in the study of those compounds that contain only rubidium and the complexant. For example, they have allowed the characterization of $Rb^+(15C5)_2,e^-$ as a pure electride and of $Rb^+(15C5)_2,Rb^-$ as a rubidide with complexed rubidium as the cation. These assignments would not have been possible with optical spectroscopy or ^{87}Rb magic angle sample spinning NMR studies. For the compound Rb(18C6), however, a final determination was not possible, and the results suggest that this stoichiometry might correspond to a mixture of species.

The alkalide and electride salts that contain $Rb^+(18C6)$ are especially difficult to crystallize, and for these, the results of this study provide the only available structural information at present. These data suggest that the conformations of 18-crown-6 in $Rb^+(18C6),Rb^-$ and in Rb(18C6) are slightly different from those in the models $Rb^+(18C6),SCN^-$ and $Rb^+(18C6),Br^-\cdot 2H_2O$, while that of $Rb^+(18C6),Na^-$ is essentially the same as those in the models. The structures of the $Rb^+(15C5)_2,X^-$ complexes are similar to that of the model compound, $Rb^+(15C5)_2,Na^-$, which has a rubidium cation sandwiched between two 15-crown-5 rings. The rubidide anion, Rb^-, has been shown to be a large anion with no nearest neighbors at detectable distances.

Acknowledgment. This work was supported by National Science Foundation Solid-State Chemistry Grants DMR 79-21979 and DMR 84-14154. CHESS is supported by NSF Grant DMR 81-12811. We gratefully acknowledge S. M. Kauzlarich for helpful discussions and S. B. Dawes, M. K. Faber, R. H. Huang, and J. Kim for their valuable assistance in collecting the data. We also thank the technical staff at CHESS for their help.

Registry No. Rb, 7440-17-7; Rb^-, 26396-76-9; RbCl, 7791-11-9; RbBr, 7789-39-1; $Rb^+(18C6),SCN^-$, 38295-06-6; $Rb^+(18C6),Br^-$, 96503-66-1; $Rb^+(15C5)_2,Na^-$, 89462-37-3; $Rb^+(15C5)_2,e^-$, 113380-65-7; $Rb^+(18C6),Na^-$, 89462-38-4; $Rb^+(15C5)_2,Rb^-$, 96503-70-7; $Rb^+(18C6),Rb^-$, 96503-68-3; Rb(18C6), 96503-72-9; $Rb^+(C2222),Rb^-$, 57450-09-6; $Rb^+(C222),e^-$, 96503-75-2; $K^+(C222),Rb^-$, 113380-66-8; $Cs^+(18C6)_2,Rb^-$, 96503-67-2; $Cs^+(15C5)_2,Rb^-$, 99582-52-2.

Singlet Molecular Oxygen: Not a Major Product of the Reaction between Tris(2,2′-bipyridine)ruthenium(3+) and Superoxide Radical Anions†

Q. G. Mulazzani,*‡ M. Ciano,‡ M. D'Angelantonio,‡ M. Venturi,‡,§ and M. A. J. Rodgers*⊥

Contribution from the Istituto di Fotochimica e Radiazioni d'Alta Energia, Consiglio Nazionale delle Ricerche, Via de' Castagnoli 1, 40126 Bologna, Italy, Dipartimento di Chimica "G. Ciamician", Via Selmi 2, 40126 Bologna, Italy, and Center for Fast Kinetics Research, University of Texas, Austin, Texas 78712. *Received September 9, 1987*

Abstract: Time-resolved infrared luminescence and computer-aided kinetic modeling have been used to demonstrate that singlet molecular oxygen, O_2 ($^1\Delta_g$), is not formed during the electron-transfer reaction between $Ru(bpy)_3^{3+}$ and $O_2^{\cdot-}$ ions in aqueous media. This is in direct contrast to what has been claimed earlier. As far as we are able to determine, the only singlet oxygen formed photolytically in a reaction mixture containing $Ru(bpy)_3^{2+}$, MV^{2+}, and O_2 is that generated by energy transfer between $^*Ru(bpy)_3^{2+}$ and ground-state oxygen. Radiolytic and electrochemical measurements have established that the bleaching of the singlet oxygen trap $ADPA^{2-}$, which occurs with a quantum yield of 0.12 ± 0.01 when H_2O or D_2O solutions containing $Ru(bpy)_3^{2+}$, MV^{2+}, O_2, and $ADPA^{2-}$ are photolyzed, is to be attributed to the oxidation of $ADPA^{2-}$ by $Ru(bpy)_3^{3+}$; from the computer modeling of the system a rate constant value of $\simeq 10^7$ $M^{-1}s^{-1}$ for the latter reaction has been evaluated.

It has been recently claimed[1] that the electron-transfer reaction between $Ru(bpy)_3^{3+}$ (bpy = 2,2′-bipyridine) and $O_2^{\cdot-}$ quantitatively generates singlet oxygen O_2 ($^1\Delta_g$) instead of the ground state O_2 ($^3\Sigma_g^-$). The two reactants were generated by the laser flash or steady-state photolysis of a system containing $Ru(bpy)_3^{2+}$, methylviologen (1,1′-dimethyl-4,4′-bipyridinium ion, MV^{2+}), and oxygen. The excitation of $Ru(bpy)_3^{2+}$ generates $^*Ru(bpy)_3^{2+}$ (reaction 1), which decays (reaction 2) with lifetimes of 0.62 and 1.02 μs in H_2O and D_2O, respectively.[2] In the absence of O_2, $^*Ru(bpy)_3^{2+}$ is quenched by MV^{2+} (reaction 3); the products of that reaction undergo electron back-transfer (reaction 4). In the

† Presented in part at the 4th International Congress on Oxygen Radicals, University of California at San Diego, LaJolla, CA, June 27–July 3, 1987.
‡ Istituto di Fotochimica e Radiazioni d'Alta Energia.
§ Dipartimento di Chimica "G. Ciamician".
⊥ Center for Fast Kinetics Research.

(1) Miller, S. S.; Zahir, K.; Haim, A. *Inorg. Chem.* **1985**, *24*, 3978–3980 and references therein.
(2) Kalyanasundaram, K. *Coord. Chem. Rev.* **1982**, *46*, 159–244.

0002-7863/88/1510-2451$01.50/0

presence of O_2 and MV^{2+}, the competitive quenching of $*Ru(bpy)_3^{2+}$ by O_2 (reaction 5) yields O_2 ($^1\Delta_g$); the efficiency of formation of O_2 ($^1\Delta_g$) via reaction 5 is 0.86 in methanol[3] and 1.0 ± 0.1 in D_2O.[1] The reaction of $MV^{\bullet+}$ with O_2 (reaction 6) generates $O_2^{\bullet-}$.

$$Ru(bpy)_3^{2+} + h\nu \rightarrow *Ru(bpy)_3^{2+} \quad (1)$$

$$*Ru(bpy)_3^{2+} \rightarrow Ru(bpy)_3^{2+} + h\nu' \quad (2)$$

$$*Ru(bpy)_3^{2+} + MV^{2+} \rightarrow Ru(bpy)_3^{3+} + MV^{\bullet+} \quad (3)$$

$$Ru(bpy)_3^{3+} + MV^{\bullet+} \rightarrow Ru(bpy)_3^{2+} + MV^{2+} \quad (4)$$

$$*Ru(bpy)_3^{2+} + O_2 \rightarrow Ru(bpy)_3^{2+} + O_2\ (^1\Delta_g) \quad (5)$$

$$MV^{\bullet+} + O_2 \rightarrow MV^{2+} + O_2^{\bullet-} \quad (6)$$

$$Ru(bpy)_3^{3+} + O_2^{\bullet-} \rightarrow Ru(bpy)_3^{2+} + O_2\ (?) \quad (7)$$

The energetics for reaction 7 are such that O_2 ($^1\Delta_g$) could indeed form. The redox potential for the Ru(III)/Ru(II) couple is 1.26 V,[2] whereas the redox potential for the $O_2/O_2^{\bullet-}$ couple is −0.33 V;[4] singlet oxygen is 0.98 eV above ground-state oxygen.[5]

The evidence for the generation of singlet oxygen via reaction 7 was obtained[1] from the photolysis of aqueous (H_2O or D_2O) solutions containing, in addition to $Ru(bpy)_3^{2+}$, MV^{2+}, and O_2, the singlet oxygen trap $ADPA^{2-}$ (9,10-anthracenedipropionate).[6] The following observations[1] were made: (i) The rate of disappearance of $ADPA^{2-}$ upon photolysis of the system at 450 nm was ca. 9-fold higher in D_2O than in H_2O. (ii) In the absence of oxygen, the rate of disappearance of $ADPA^{2-}$ was less than 1% of that observed in the presence of oxygen. (iii) From an assumed mechanism based on reactions 1–3 and 6–9, a yield of singlet oxygen from reaction 7 of 1.2 ± 0.2 was calculated. The quantitative formation of singlet oxygen in reaction 7 at the expense of the thermodynamically more favorable formation of ground-state oxygen was tentatively attributed to the nonadiabaticity of reaction 7 (when it generates ground-state oxygen) or to the inverted region effect.[1]

Chemical traps for singlet oxygen (e.g., $ADPA^{2-}$) are unfortunately not unambiguous in their effect. On the other hand, the infrared luminescence (IRL) at 1.27 μm resulting from the weakly allowed transition (reaction 8) is specific and unambiguous.

$$O_2\ (^1\Delta_g) \rightarrow O_2\ (^3\Sigma_g^-) + h\nu'' \quad (8)$$

$$O_2\ (^1\Delta_g) + ADPA^{2-} \rightarrow (ADPA)O_2^{2-} \quad (9)$$

Preliminary experiments that we performed on this system using IRL indicated that singlet oxygen was not generated to an appreciable extent by reaction 7. In order to clarify the origin of this unexpected discrepancy, we have reinvestigated reaction 7 and related processes with the use of continuous and laser flash photolysis, continuous radiolysis, and cyclic voltammetry.

Experimental Section

Materials. $[Ru(bpy)_3]Cl_2 \cdot 6H_2O$ (Carlo Erba) was used as received or was transformed into the perchlorate salt. Samples of 9,10-anthracenedipropionic acid ($ADPAH_2$) and its conjugated base ($ADPA^{2-}$) in the form of the disodium salt were available from a previous study.[6] Methylviologen dichloride (Aldrich), sodium formate and sodium chloride (Merck), potassium bromide and lithium chloride (Merck, Suprapur), deuterium oxide (Aldrich, 99.8 atom %), and acetonitrile (Carlo Erba, polarography grade) were used as received. The water was purified by passage through a Millipore purification train. The solutions were saturated with O_2 or with purified N_2O, purged with Ar or N_2, or degassed by standard vacuum line techniques. If not otherwise stated, the solutions were at their natural pH and μ = 0.2 M (adjusted with NaCl).

Procedures. Laser flash photolysis experiments using kinetic spectrophotometric (absorption or emission) detection were performed at the Center for Fast Kinetics Research (CFKR), University of Texas at Austin, where Q-switched Nd:YAG lasers were used to generate pulses of 11-ns duration.[7] If not otherwise stated, the excitation wavelength was 355 nm. Kinetic data were obtained from the computer averaging of 10–20 individual shots. The singlet oxygen infrared emission measurements were also carried out at CFKR according to the procedures previously described.[8,9]

Continuous photolysis experiments were carried out at the Dipartimento di Chimica "G. Ciamician", Bologna, with a medium-pressure Hg lamp (Hanau Q 400) equipped with an interference filter with T_{max} = 0.55 at 436 nm. Solutions were contained in a 1-cm cuvette and were stirred by bubbling oxygen during the irradiation. The intensity of light incident on the solutions was determined by means of ferrioxalate actinometry.[10] The absorption spectra, taken after fixed (30-s) irradiation times, were recorded with a Kontron Uvikon 860 spectrophotometer.

Continuous radiolysis experiments, carried out at the FRAE Institute of CNR, Bologna, were performed on 10-mL samples contained in silica or Pyrex vessels that were provided with silica optical cells on a side arm. Absorption spectra were recorded with Perkin-Elmer Model 555 or Lambda 5 spectrophotometers. The radiation sources were two ^{60}Co-Gammacells (AEC, Ltd.) with dose rates of ca. 6.3 and ca. 123 Gy min^{-1}, respectively. The absorbed radiation dose was determined with the Fricke chemical dosimeter, taking $G(Fe^{3+})$ = 15.5, where $G(X)$ = number of molecules of species X formed per 100 eV of energy absorbed by the solution.

Electrochemistry. Cyclic voltammetry was performed with an Amel 448 oscillographic polarograph on Ar-purged acetonitrile solutions or mixtures of acetonitrile and water (95/5, v/v) containing 0.05 M tetraethylammonium tetrafluoroborate ($(TEA)BF_4$) as a supporting electrolyte. The working electrode was a glassy carbon electrode, the counter electrode was a platinum wire, and a standard calomel electrode (SCE) was the reference electrode. After the establishment of the correct working conditions by the cyclic voltammograms, controlled-potential electrolyses were performed with an Amel Model 563 Electrochemolab equipment. The spectra of electrochemically generated species were obtained at a Pt–Rh grid used as an OTTLE (optical transparent thin-layer electrode) placed between the windows of a 2-mm spectrophotometric cell directly mounted in a Kontron Uvikon 860 spectrophotometer. The counter electrode was a Pt wire separated from the anodic compartment by a fine frit; an Ag wire acted as a quasi reference electrode.

Radiolytic Generation of Radicals. The radiolysis of aqueous solutions generates e_{aq}^-, $OH^\bullet$ radicals, $H^\bullet$ atoms, and molecular products (H_2, H_2O_2) according to eq 10 where the numbers in parentheses represent

$$H_2O \rightsquigarrow e_{aq}^-\ (2.8),\ OH^\bullet\ (2.8),\ H^\bullet(0.6),\ H_2\ (0.45),\ H_2O_2\ (0.8) \quad (10)$$

the G values for the individual species. In N_2O-saturated (25 mM) solution, e_{aq}^- is converted to $OH^\bullet$ according to reaction 11; in O_2-saturated (1.25 mM) solution, e_{aq}^- is converted to $O_2^{\bullet-}$ according to reaction 12. $O_2^{\bullet-}$ is in equilibrium with its conjugated acid $HO_2^\bullet$ (reaction 13)

$$e_{aq}^- + N_2O + H_2O \rightarrow N_2 + OH^\bullet + OH^- \quad (11)$$

$$k = 8.7 \times 10^9\ M^{-1}\ s^{-1}\ (\text{ref } 11)$$

$$e_{aq}^- + O_2 \rightarrow O_2^{\bullet-} \quad (12)$$

$$k = 1.9 \times 10^{10}\ M^{-1}\ s^{-1}\ (\text{ref } 11)$$

for which pK_a = 4.8.[12] In the presence of HCO_2^- (0.1 M), reaction 14 takes place; if the solution is saturated with oxygen, reaction 15 takes

$$HO_2^\bullet \rightleftharpoons H^+ + O_2^{\bullet-} \quad (13)$$

$$H^\bullet/OH^\bullet + HCO_2^- \rightarrow H_2/H_2O + CO_2^{\bullet-} \quad (14)$$

$$k = 3 \times 10^8/3 \times 10^9\ M^{-1}\ s^{-1}\ (\text{ref } 13 \text{ and } 14)$$

$$CO_2^{\bullet-} + O_2 \rightarrow CO_2 + O_2^{\bullet-} \quad (15)$$

$$k = 2.4 \times 10^9\ M^{-1}\ s^{-1}\ (\text{ref } 12)$$

(3) Hauenstein, B. L., Jr.; Dressick, W. J.; Buell, S. L.; Demas, J. N.; DeGraff, B. A. *J. Am. Chem. Soc.* **1983**, *105*, 4251–4255.
(4) (a) Wood, P. M. *FEBS Lett.* **1974**, *44*, 22–24. (b) Ilan, Y. A.; Meisel, D.; Czapski, G. *Isr. J. Chem.* **1974**, *12*, 891–895. (c) Berdnikov, V. M.; Zhuravleva, O. S. *Russ. J. Phys. Chem.* **1972**, *46*, 1521–1523.
(5) For a detailed list of references on singlet oxygen see: Gorman, A. A.; Rodgers, M. A. J. *Chem. Soc. Rev.* **1981**, *10*, 205–231.
(6) Lindig, B. A.; Rodgers, M. A. J.; Schaap, A. P. *J. Am. Chem. Soc.* **1980**, *102*, 5590–5593.
(7) Foyt, D. C. *Comput. Chem.* **1981**, *5*, 49.
(8) Rodgers, M. A. J.; Snowden, P. T. *J. Am. Chem. Soc.* **1982**, *104*, 5541–5543.
(9) Rodgers, M. A. J. *J. Am. Chem. Soc.* **1983**, *105*, 6201–6205.
(10) Hatchard, C. G.; Parker, C. A. *Proc. R. Soc. London Ser. A* **1950**, *235*, 518–536.
(11) Anbar, M.; Bambenek, M.; Ross, A. B. *Natl. Stand. Ref. Data Ser. (U.S. Natl. Bur. Stand.)* **1973**, *No. 43*.
(12) Bielski, B. H. J.; Cabelli, D. E.; Arudi, R. L.; Ross, A. B. *J. Phys. Chem. Ref. Data* **1985**, *14*, 1041–1100 and references therein.
(13) Anbar, M.; Farhataziz; Ross, A. B. *Natl. Stand. Ref. Data Ser. (U.S. Natl. Bur. Stand.)* **1975**, *No. 51*.
(14) Farhataziz; Ross, A. B. *Natl. Stand. Ref. Data Ser. (U.S. Natl. Bur. Stand.)* **1977**, *No. 59*.

Table I. Kinetic Parameters of the Reactions Induced by the Photoillumination of Aqueous (H_2O, D_2O) Solutions Containing $Ru(bpy)_3^{2+}$, MV^{2+}, and O_2

no.	reaction	rate constants: computer modeling	rate constants: literature
2	$^*Ru(bpy)_3^{2+} \rightarrow Ru(bpy)_3^{2+} + h\nu'$	1.0×10^6 s^{-1} [a,b] 1.6×10^6 s^{-1} [a,c]	
3	$^*Ru(bpy)_3^{2+} + MV^{2+} \rightarrow Ru(bpy)_3^{3+} + MV^{\bullet+}$	1.3×10^9 M^{-1} s^{-1} [d,e]	$(1.0 \pm 0.2) \times 10^9$ M^{-1} s^{-1} [l,m]
5	$^*Ru(bpy)_3^{2+} + O_2 \rightarrow Ru(bpy)_3^{2+} + {}^1O_2$	3.7×10^9 M^{-1} s^{-1} [d,f]	3×10^9 M^{-1} s^{-1} [l]
6	$MV^{\bullet+} + O_2 \rightarrow MV^{2+} + O_2^{\bullet-}$	6.0×10^8 M^{-1} s^{-1} [d,g]	$(8.1 \pm 0.7) \times 10^8$ M^{-1} s^{-1} [l,m] $(8.0 \pm 0.3) \times 10^8$ M^{-1} s^{-1} [n]
7	$Ru(bpy)_3^{3+} + O_2^{\bullet-} \rightarrow Ru(bpy)_3^{2+} + O_2$	8.0×10^9 M^{-1} s^{-1} [d,h]	$(1.43 \pm 0.03) \times 10^{10}$ M^{-1} s^{-1} [l,o]
8	$^1O_2 \rightarrow {}^3O_2 + h\nu''$	1.7×10^4 s^{-1} [d,i]	$(1.9 \pm 0.1) \times 10^4$ s^{-1} [p,q]
18	$O_2^{\bullet-} + O_2^{\bullet-} \xrightarrow{2H^+} O_2 + H_2O_2$	1.0×10^6 M^{-1} s^{-1} [j,k]	

[a] Reference 2. [b] In D_2O. [c] In H_2O. [d] This work. [e] In H_2O and D_2O at $\mu = 0.2$. [f] In H_2O and D_2O, independent of μ between $\simeq 0$ and 0.2. [g] In H_2O, independent of μ between $\simeq 0$ and 1.0. [h] In D_2O, at natural pH and $\mu = 0.2$. [i] In D_2O, at $\mu = 0.2$. [j] Reference 12. [k] In H_2O, at pH 7. [l] Reference 1. [m] In H_2O, at $\mu = 0.1$. [n] Reference 20. [o] In H_2O, at pH ≥ 7 and $\mu = 0.1$. [p] Reference 6. [q] In D_2O, natural ionic strength.

place so that $O_2^{\bullet-}$ is the major reacting species produced in the system. In the presence of Br^- (0.1 M), $OH^\bullet$ radicals are converted to $Br_2^{\bullet-}$ radicals according to reaction 16; thus, in N_2O-saturated solution con-

$$OH^\bullet + Br^- \xrightarrow{Br^-} OH^- + Br_2^{\bullet-} \qquad (16)$$

taining Br^-, the reactive species is the $Br_2^{\bullet-}$ radical only, whereas in O_2-saturated solution the reactive species are $O_2^{\bullet-}/HO_2^\bullet$ and $Br_2^{\bullet-}$. The redox potentials of the $CO_2/CO_2^{\bullet-}$ and $Br_2^{\bullet-}/2Br^-$ couples are -2.0[15] and 1.69 V,[16] respectively.

Computer Analysis. The differential equations describing the reaction mechanisms were numerically integrated with the use of a program based on that of Hindmarsh[17] and a Gould Sel Computer 27/32.

Results

Laser Flash Photolysis Experiments. By following the emission of $^*Ru(bpy)_3^{2+}$ at 620 nm,[2] or the changes in absorbance at 450 nm, where $\epsilon(Ru(bpy)_3^{2+})$ and $\epsilon(Ru(bpy)_3^{3+})$ are 14 500 and 1500 M^{-1} cm^{-1},[2] respectively, and at 600 nm, where $\epsilon(MV^{\bullet+}) = 1.37 \times 10^4$ $M^{-1}cm^{-1}$,[18] we could determine the rate constants of the reactions taking place when solutions containing $Ru(bpy)_3^{2+}$, MV^{2+}, and O_2 were flash photolyzed. Specifically, $k_3 = 1.3 \times 10^9$ M^{-1} s^{-1} in H_2O and D_2O at $\mu = 0.2$ M; $k_5 = 3.7 \times 10^9$ M^{-1} s^{-1} in H_2O and D_2O solutions, independent of ionic strength in the range 0–0.2 M; $k_6 = 6.0 \times 10^8$ M^{-1} s^{-1} in H_2O, independent of ionic strength in the range 0–1.0 M. The uncertainty in these values, which are compared with literature values in Table I, is estimated to be ±10%.

The reaction between $Ru(bpy)_3^{3+}$ and $O_2^{\bullet-}$ (reaction 7) was monitored at 450 nm by following the recovery of the absorption of $Ru(bpy)_3^{2+}$. The process strictly followed a second-order rate law (Figure 1). The slope ($=k_7/\Delta\epsilon l$) decreased with increasing ionic strength, as expected for a reaction between oppositely charged species. At a fixed ionic strength of 0.2 M in O_2-saturated D_2O solutions, the slope was unaffected by a change in $[MV^{2+}]$ (5–50 mM) (Figure 1, inset). By taking $\Delta\epsilon = 13\,000$ M^{-1} cm^{-1} at 450 nm and $l = 0.35$ cm, where l represents the length of the excited region along the path of the analyzing light, a value of $k_7 = 8.0 \times 10^9$ M^{-1} s^{-1} was calculated with an uncertainty of ca. 20%. The value of k_7 given in ref 1 is $(1.43 \pm 0.03) \times 10^{10}$ M^{-1} s^{-1} at $\mu = 0.1$ M and pH ≥ 7. At lower pH's, the value of k_7 decreased sharply[1] due to the protonation of $O_2^{\bullet-}$ to form $HO_2^\bullet$ (reaction 13); the results of control experiments we performed in acidic solutions were fully consistent with this finding.

From the amount of bleaching at 450 nm and the amount of absorbance of $MV^{\bullet+}$ at 600 nm obtained under conditions in which ≥90% of $^*Ru(bpy)_3^{2+}$ was quenched by MV^{2+}, the concentrations of $Ru(bpy)_3^{3+}$ and $O_2^{\bullet-}$ observed immediately after the laser pulse were estimated to be ca. 8–10 μM.

Singlet Oxygen Infrared Emission Measurements. These experiments were performed on the same set of solutions that were used for the determination of k_7 and the same laser conditions.

In the absence of MV^{2+}, in O_2-saturated D_2O solutions, the trace shown in Figure 2 was obtained. In the presence of MV^{2+}, the singlet oxygen emission was seen to decrease with increasing $[MV^{2+}]$ as is shown in Figure 3 where the intensity of emission, in arbitrary units, extrapolated to zero time is reported as a function of $[MV^{2+}]$. Since the decay is strictly exponential with a constant lifetime of 60 ± 3 μs (Figure 3, inset), the emission intensity values reported in Figure 3 are proportional to the concentration of singlet oxygen. When a solution containing 5.0 mM MV^{2+} was made acidic with one drop of concentrated HCl, the emission intensity was unaffected but the lifetime decreased by about 15%.

The data shown in Figure 3 generated the Stern–Volmer type plot shown in Figure 4a (solid line) from which a value of 208 M^{-1} for the slope was obtained.

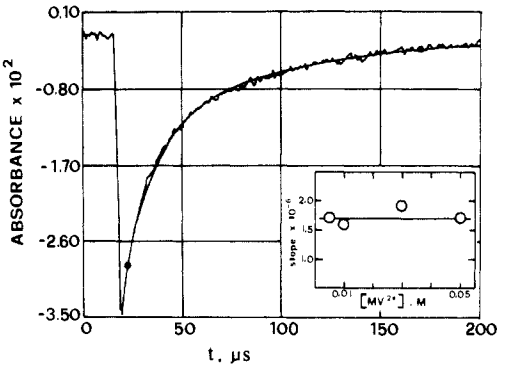

Figure 1. Recovery of absorbance at 450 nm associated with the reduction of $Ru(bpy)_3^{3+}$ by $O_2^{\bullet-}$ as obtained from the laser flash photolysis of a D_2O solution saturated with O_2, containing 55 μM $Ru(bpy)_3^{2+}$ and 50 mM MV^{2+}. The solid line represents the curve calculated according to a second-order rate law. Inset: values of slope = $k/\Delta\epsilon l$ as a function of $[MV^{2+}]$.

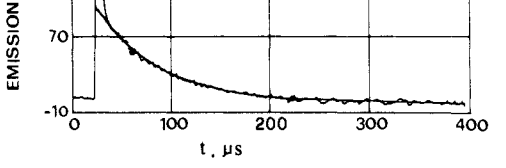

Figure 2. Infrared emission from the laser flash photolysis of a D_2O solution saturated with O_2, containing 55 μM $Ru(bpy)_3^{2+}$. The intense early component, which is complete within $\simeq 5$ μs, is probably luminescence from $^*Ru(bpy)_3^{2+}$ that has weak, but significant, intensity at wavelengths passed by the filter (>1.1 μm).

(15) Breitenkamp, M.; Henglein, A.; Lilie, J. *Ber. Bunsenges. Phys. Chem.* **1976**, *80*, 973–977.
(16) Endicott, J. F. In *Concept of Inorganic Photochemistry*; Adamson, A. W., Fleishauer, P. D., Eds.; Wiley: New York, 1975; p 88.
(17) Hindmarsh, A. C. "GEAR:Ordinary Differential Equation System Solver"; LLNL Report UCID 30001, Rev. 3, Dec 1974.
(18) Watanabe, T.; Honda, K. *J. Phys. Chem.* **1982**, *86*, 2617–2619.

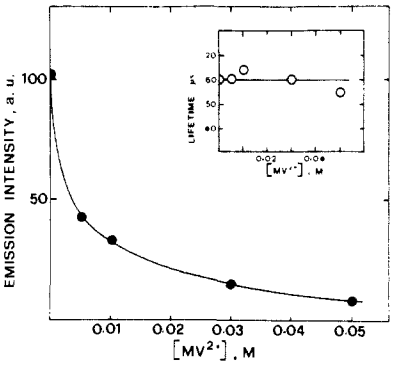

Figure 3. Infrared emission intensity vs $[MV^{2+}]$ as obtained from the laser flash photolysis of D_2O solutions saturated with O_2, containing 55 μM $Ru(bpy)_3^{2+}$. Inset: lifetime of the infrared emission (obtained from the kinetic analysis of traces such as that shown in Figure 2) as a function of $[MV^{2+}]$.

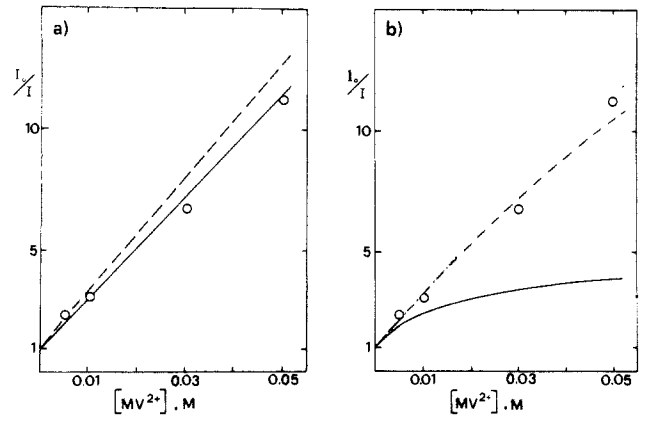

Figure 4. (a) Stern–Volmer type plots: obtained from the data shown in Figure 3 (solid line); calculated (see text) for $\alpha = 0$ (broken line). (b) Calculated Stern–Volmer type plots: (•••) $\alpha = 0.05$; (–·–) $\alpha = 0.1$; (—) $\alpha = 1.0$.

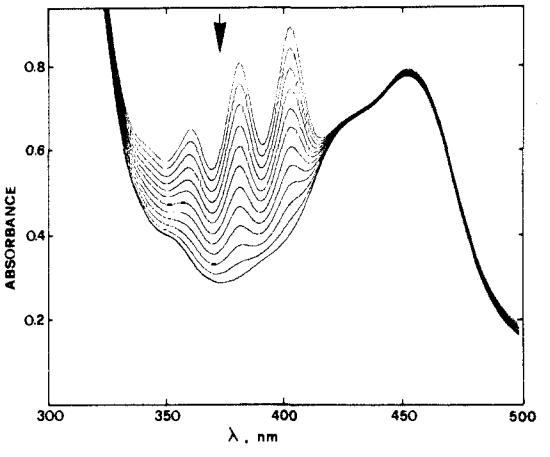

Figure 5. Spectral changes induced by the continuous photolysis of a D_2O solution saturated with O_2, containing 50 μM $Ru(bpy)_3^{2+}$, 50 mM MV^{2+}, and 70 μM $ADPA^{2-}$; optical path 1.0 cm. The arrow indicates the direction of the changes. Very similar spectral changes were observed when D_2O was replaced by H_2O.

Continuous Photolysis Experiments. The photolysis ($\lambda = 436$ nm) of O_2-saturated solutions containing 50 μM $Ru(bpy)_3^{2+}$, 50 mM MV^{2+}, and 70 μM $ADPA^{2-}$ at natural pH and $\mu = 0.2$ M resulted in the disappearance of the absorption due to $ADPA^{2-}$ (Figure 5). In contrast with the observations reported in ref 1, however, the rate of disappearance of $ADPA^{2-}$ was virtually the same in both D_2O and H_2O solutions and corresponded to a quantum yield of 0.12 ± 0.01. This latter value was calculated taking $\epsilon = 7500 \pm 500$ M^{-1} cm^{-1} for $ADPA^{2-}$ at 378 nm. The use of the latter value for this calculation, instead of 11 500 M^{-1} cm^{-1},[1] was dictated by the fact that the presence of 50 mM MV^{2+} decreased the absorption of $ADPA^{2-}$ by about 35–40%, presumably due to the formation of an ion pair. No absorption at 436 nm was detected from solutions containing $ADPA^{2-}$ and MV^{2+} only.

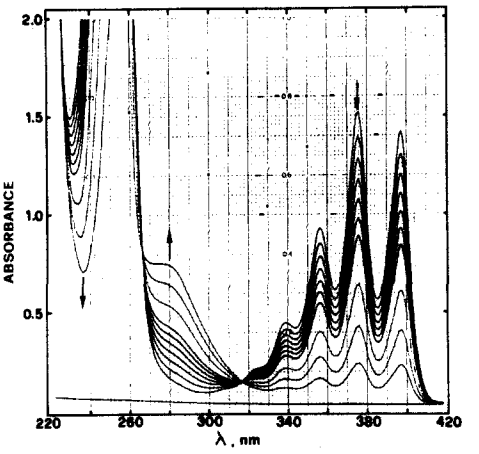

Figure 6. Spectral changes induced by the continuous radiolysis of an O_2-saturated aqueous solution containing 125 μM $ADPA^{2-}$ and 0.1 M KBr; optical path 1.0 cm. The spectra refer to absorbed doses of 0, 14.8, 29.6, 44.4, 59.2, 74.0, 88.8, 131.4, 174.0, and 216.6 Gy, respectively. The arrows indicate the direction of the changes.

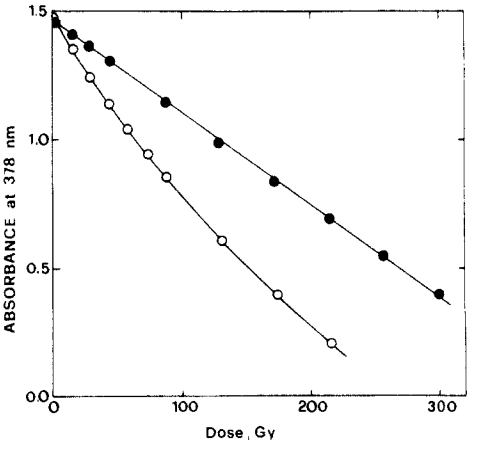

Figure 7. Changes of absorbance at 378 nm vs dose as induced by the continuous radiolysis of aqueous solutions containing 125 μM $ADPA^{2-}$ and 0.1 M KBr at pH 7: (○) O_2-saturated solution; (●) N_2O-saturated solution.

Table II. Effect of $[ADPA^{2-}]_0$ and Dose Rate on $G(-ADPA^{2-})$[a]

$[ADPA^{2-}]_0$, μM	dose rate, Gy min^{-1}	$G(-ADPA^{2-})$
18.7	6.3	3.6
127.0	6.3	7.5
187.0	6.3	9.3
187.0	121.1	5.3

[a] Extrapolated to zero dose.

Continuous Radiolysis Experiments. When an aqueous solution, saturated with O_2 at pH 7.0 and containing 50 μM $ADPA^{2-}$ and 0.1 M HCO_2^-, was irradiated with a dose of ca. 100 Gy, its spectrum did not show any appreciable change. In contrast, the irradiation of an O_2-saturated solution containing 125 μM $ADPA^{2-}$ and 0.1 M KBr at natural pH caused the spectral changes shown in Figure 6. Specifically, the absorbance of $ADPA^{2-}$ in the 230–270- and 320–420-nm regions decreased with increasing dose, and a new band formed at ca. 280 nm; two clean isosbestic points at 266 and 316 nm were observed. As is shown in Figure 7, the decrease of the absorbance at 378 nm was not linear with the dose, demonstrating that the value of $G(-ADPA^{2-})$ decreases with increasing dose and equals 7.5 when extrapolated to zero dose. Table II summarizes the dependence of $G(-ADPA^{2-})$, extrapolated

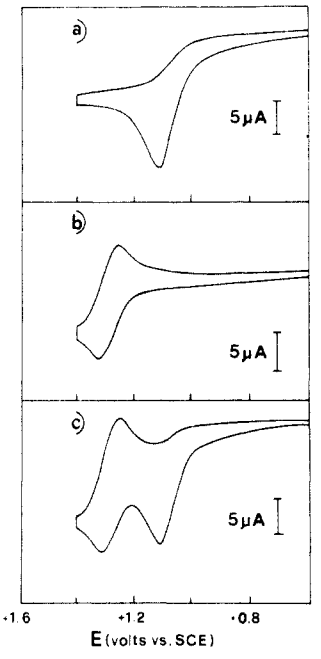

Figure 8. Cyclic voltammetry on glassy carbon electrode of Ar-purged CH_3CN solutions containing (a) 0.52 mM $ADPAH_2$, (b) 0.52 mM $[Ru(bpy)_3](ClO_4)_2$, and (c) 0.52 mM each $ADPAH_2$ and $[Ru(bpy)_3](ClO_4)_2$ in the presence of 0.05 M $(TEA)BF_4$; scan rate 0.04 V/s.

to zero dose, on dose–rate and $[ADPA^{2-}]_0$.

When the solution containing 125 μM $ADPA^{2-}$ and 0.1 M KBr was saturated with N_2O instead of O_2, the rate of disappearance of $ADPA^{2-}$ was lower and independent of dose up to at least 50% conversion of $ADPA^{2-}$ (Figure 7). Under these conditions, $G(-ADPA^{2-}) = 2.9 \pm 0.1$.

Cyclic Voltammetry Measurements. The cyclic voltammograms of Ar-purged acetonitrile solutions containing, in addition to 0.05 M $(TEA)BF_4$, 0.52 mM $ADPAH_2$, 0.52 mM $[Ru(bpy)_3](ClO_4)_2$, or 0.52 mM $ADPAH_2$ and $[Ru(bpy)_3](ClO_4)_2$ are shown in Figure 8. $ADPAH_2$ shows only an anodic peak at 1.10 V (Figure 8a), whereas $Ru(bpy)_3^{2+}$ shows an anodic peak at 1.30 V and a reversal cathodic peak at 1.24 V (Figure 8b); this latter voltammogram matches very closely one previously reported.[19] The voltammogram of the solution containing both species (Figure 8c) corresponds to a composite of their individual voltammograms.

The controlled-potential electrolysis at 1.2 V vs AgRE on the Pt–Rh minigrid electrode of an Ar-purged acetonitrile solution containing 0.52 mM $ADPAH_2$ and 0.05 M $(TEA)BF_4$ caused the disappearance of the absorption of $ADPAH_2$. A value of $n_{app} = 1.9 \pm 0.2$ was calculated, where n_{app} represents the number of faradays per mole of $ADPAH_2$. A similar value of n_{app} was obtained from the controlled-potential electrolysis of an identical solution saturated with oxygen.

Due to the insolubility of $ADPA^{2-}$ in neat acetonitrile, the cyclic voltammetry for the latter species was performed by using a mixture (95/5, v/v) of acetonitrile and water. The voltammogram obtained under these conditions was very similar to the one obtained for $ADPAH_2$ in neat acetonitrile, except that the anodic peak was shifted toward less positive potentials by ca. 60 mV. A similar shift, as compared with the neat acetonitrile conditions, was observed when the cyclic voltammetry was performed with $Ru(bpy)_3^{2+}$ in the same mixed solvent.

Discussion

We note, first of all, that the rate parameters that we have obtained from the laser flash photolysis experiments performed on solutions containing $Ru(bpy)_3^{2+}$, MV^{2+}, and O_2 are in substantial agreement with those described in ref 1. The singlet oxygen infrared emission measurements, however, rule out the possibility that a significant amount of singlet oxygen is generated by reaction 7. As far as we can tell, the singlet oxygen emission we have detected originates from reaction 5 only. In fact, the intensity and decay profiles of the singlet oxygen emission in solutions containing MV^{2+} were not affected by adding hydrochloric acid. Were reaction 7 a pathway for producing significant yields of O_2 ($^1\Delta_g$), then converting $O_2^{\bullet-}$ to its conjugate acid $HO_2^{\bullet}$ would have profoundly affected the luminescence parameters since, in agreement with Miller et al.,[1] we observed that the recombination process is orders of magnitude less efficient in an acidic medium.

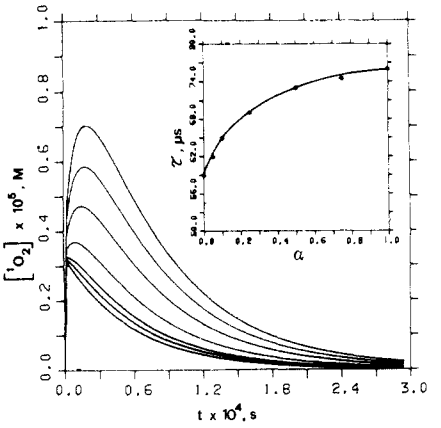

Figure 9. Calculated (see text) concentration of singlet oxygen as a function of time as obtained from the computer modeling of the system when subjected to laser flash photolysis. Conditions assumed: 50 μM $^*Ru(bpy)_3^{2+}$, 50 mM MV^{2+}, O_2-saturated D_2O solution. Top to bottom: $\alpha = 1.0, 0.75, 0.5, 0.25, 0.1, 0.05$, and 0.0, respectively. Inset: calculated lifetime of singlet oxygen as a function of α.

Quantitative evidence against reaction 7 being a significant source of singlet oxygen is represented by the fact that the singlet oxygen emission intensity at $t = 0$ decreases with increasing $[MV^{2+}]$ in a way that is insignificantly different from that predicted by a calculation based on the competition between reactions 2, 3, and 5. This leads to

$$I_0/I = 1 + k_3[MV^{2+}]/(k_2 + k_5[O_2])$$

with I_0 and I representing the amplitudes of the infrared luminescence extrapolated to zero time (e.g., as depicted in Figure 2) in the absence and presence of MV^{2+}, respectively. Substituting the literature value for k_2 (in D_2O solution), using either our own values for k_3 and k_5 (Table I) or those of Miller et al.[1] (also in Table I), and taking $[O_2] = 1.25 \times 10^{-3}$ M, we obtain calculated slopes for the Stern–Volmer type plot (Figure 4a) of 238 M^{-1} (our k_3 and k_5) and 217 M^{-1} (k_3 and k_5 from ref 1). These compare with 208 M^{-1} obtained experimentally (Figure 4a). Furthermore, the decay of the infrared luminescence signal was always exponential with a time constant that was invariant with MV^{2+} concentration (Figure 3, inset). Hence the product $I\tau_\Delta$, which is proportional to the total number of O_2 ($^1\Delta_g$) species produced, from whatever sources, subsequent to the laser pulse, changes with $[MV^{2+}]$ identically as I changes. These considerations strongly suggest that singlet oxygen luminescence in the experimental system arises solely from the energy-transfer process 5.

This conclusion is supported by a computer modeling of the time variance of the singlet oxygen concentration. In this exercise we have used reaction 7a to summarize the detailed results of the

$$Ru(bpy)_3^{3+} + O_2^{\bullet-} \rightarrow Ru(bpy)_3^{2+} + \alpha\Delta + (1-\alpha)\Sigma \qquad (7a)$$

recombination process. In (7a), α represents the fraction of the recombination reactions that yield Δ (singlet oxygen) and was used as a variable parameter yielding a family of curves (Figure 9). The modeling procedure included reactions 2, 3, and 5–8 for the initial conditions where $[MV^{2+}] = 50$ mM. The energy-transfer (reaction 5) and cage-escape (reaction 3) efficiencies were

(19) Tokel-Takvoryan, N. E.; Hemingway, R. E.; Bard, A. J. *J. Am. Chem. Soc.* **1973**, *95*, 6582–6589.
(20) Farrington, J. A.; Ebert, M.; Land, E. J. *J. Chem. Soc., Faraday Trans 1* **1978**, *74*, 665–675.

taken as 1.0 and 0.21, respectively.[1] The calculated curves (Figure 9) predict a departure from exponentiality in the singlet oxygen concentration due to the fact that, with increasing α, increasing amounts of singlet oxygen would be formed at a rate governed by the second-order reaction (7). This would induce a departure from exponentiality in the singlet oxygen decay. In a similar manner, for constant α, increasing amounts of MV^{2+} would increasingly compete with the energy-transfer route (reaction 5) so that an enhanced departure from exponentiality would occur. To estimate this departure from exponentiality in the singlet oxygen decay, the lifetimes of the singlet oxygen were calculated by neglecting the initial part ($\simeq 30$ μs) of the traces such as those shown in Figure 9 and by assuming exponential behavior for the remaining part. For a fixed $[MV^{2+}]$, these calculated lifetimes increase with increasing α in the way shown in the inset of Figure 9, which refers to $[MV^{2+}] = 50$ mM. Our luminescence data showed no tendencies to mirror the $\alpha \neq 0$ curves in Figure 9, nor was any singlet oxygen lifetime increase detected (Figure 3, inset).

The time variance plots that were used for calculating the singlet oxygen lifetimes (Figure 9) allowed us to estimate the values of the intensity of the infrared emission at zero time for the cases in which α was different from zero. These lead, in Figure 4b, to the Stern–Volmer type plots based on values of α of 0.05, 0.1, and 1, respectively.

Taken together the above three points (coincidence of experimental and calculated Stern–Volmer coefficients; shapes of the computer-modeled time variances; Stern–Volmer presentations of the intensities of the computer-modeled time variances) are the source of our assertion that $\alpha = 0$ or is so close to zero that O_2 ($^1\Delta_g$) produced by reaction 7 is lost in the random error.

Despite the inefficiency of reaction 7 in generating singlet oxygen and in agreement with the results reported in ref 1, we have observed that $ADPA^{2-}$ is bleached when the system containing $Ru(bpy)_3^{2+}$, MV^{2+}, O_2, and $ADPA^{2-}$ is photolyzed. In net contrast with the findings reported in ref 1, however, we were unable to detect any significant difference between the rate of disappearance of $ADPA^{2-}$ in D_2O and in H_2O, a fact that casts doubt that the bleaching of $ADPA^{2-}$ observed under these conditions results from singlet oxygen reaction. We were therefore forced to search for an explanation for the disappearance of $ADPA^{2-}$ not based on the intervention of singlet oxygen.

The radiolytic experiments have shown that strong oxidants such as $Br_2^{\bullet-}$ cause the bleaching of the $ADPA^{2-}$ absorption in the visible–near-UV region. Furthermore, in O_2-saturated solution, the bleaching of the absorbance of $ADPA^{2-}$ is higher (factor of 2–3) than the one obtained in the presence of N_2O. This fact leads us to suggest that the radiolytically induced oxidation of $ADPA^{2-}$ takes place, in the presence of oxygen, according to a chain-reaction mechanism. This will be discussed in more detail later.

In agreement with the radiolytic results, the electrochemical experiments have shown that the controlled-potential oxidation of $ADPA^{2-}$ causes the bleaching of its visible–near-UV absorption. The electrochemical measurements have also shown that $Ru(bpy)_3^{3+}$ is thermodynamically capable of oxidizing $ADPA^{2-}$ (reaction 17) and therefore may be responsible for the $ADPA^{2-}$ bleaching observed here and by Miller et al.[1] under continuous photolysis conditions. If k_{17} is of significant magnitude, reaction 17 can compete favorably with reaction 7 since the latter is kinetically second order and therefore, under continuous illumination, it will be inefficient. We examined this possibility by the computer modeling of a reaction mechanism consisting of reactions 1–3, 5–7, 17, and 18, using the rate constants reported in Table I. The conditions chosen corresponded to the experimental ones (Figure 5) where the rate of formation of $^*Ru(bpy)_3^{2+}$ was 1.95×10^{-6} M s^{-1}. As before, it was assumed that the yield for the formation of singlet oxygen from reaction 5 and the cage separation yield from $Ru(bpy)_3^{3+}|MV^{\bullet+}$ are 1.0 and 0.21, respectively. It was also assumed that, under photolytic conditions, the same chain-reaction mechanism detected under radiolytic conditions was taking place. In other words, it was assumed that the observed (0.12 ± 0.01) quantum yield for $ADPA^{2-}$ disappearance originated from a quantum yield for $ADPA^{\bullet-}$ formation (reaction 17 in competition with reaction 7) of 0.06. A satisfactory fitting of the rate of disappearance of $ADPA^{2-}$ was obtained by using $k_{17} \simeq 10^7$ M^{-1} s^{-1}. Although originated from a calculation ignoring many details of the reaction mechanism such as those related to the chain reaction, the estimate of k_{17} seems reasonable in terms of the difference observed between the values of E_{pa} for $Ru(bpy)_3^{2+}$ and $ADPA^{2-}$ which amounts to 200 mV.

$$Ru(bpy)_3^{3+} + ADPA^{2-} \rightarrow Ru(bpy)_3^{2+} + ADPA^{\bullet-} \quad (17)$$

$$O_2^{\bullet-} + O_2^{\bullet-} \xrightarrow{2H^+} O_2 + H_2O_2 \quad (18)$$

In conclusion, we attribute the photoinduced disappearance of $ADPA^{2-}$ from the system examined to the oxidation of $ADPA^{2-}$ itself by $Ru(bpy)_3^{3+}$.

Radiolysis of the $ADPA^{2-}$–KBr System. In N_2O-saturated solution $G(-ADPA^{2-}) = {}^1/_2G(Br_2^{\bullet-})$, thus indicating that the product of the oxidation of $ADPA^{2-}$ by $Br_2^{\bullet-}$ (reaction 19) disproportionates according to reaction 20, where $ADPA^0$ represents generically the two-electron-oxidized species. Most likely, the same two-electron-oxidized species is directly obtained upon electrochemical oxidation of $ADPAH_2$ and $ADPA^{2-}$ in acetonitrile and acetonitrile/water mixture, respectively, as is suggested by the lack of a reversal cathodic peak, the height of the anodic peak, which is about twice that obtained with $Ru(bpy)_3^{2+}$, and the value of n_{app} ($\simeq 2$). Surprisingly, although depending upon the dose, the dose rate, and $[ADPA^{2-}]_0$, the value of $G(-ADPA^{2-})$ obtained in the presence of oxygen is higher (factor of 2–3) than that obtained in the presence of N_2O. In O_2-saturated solution, $G(Br_2^{\bullet-})$ is ca. half of that obtained in N_2O-saturated solution so that a value of $G(-ADPA^{2-})$ of the order of 1.5 would be expected if the mechanism of $ADPA^{2-}$ oxidation were the same in O_2- and N_2O-saturated solutions. The experiments performed in the presence of HCO_2^- and O_2 have shown that $O_2^{\bullet-}$ does not interact with $ADPA^{2-}$. The data collected in Table II are consistent with a chain-reaction mechanism represented by Scheme I. Here, the initiation step is represented by reaction 21 and the propagation step by reaction 22; reactions 20, 23, and 24 represent the possible termination steps. Since the chain length is small, the initiation and/or the propagation steps are rather inefficient in comparison with the termination step(s). The fact that the chain mechanism does not take place when $ADPAH_2$ is oxidized electrochemically (the same value for n_{app} was obtained in O_2-saturated and Ar-purged solutions) is consistent with the view that, at the electrode, the oxidation of $ADPAH_2$ is a one-step two-electron process.

$$ADPA^{2-} + Br_2^{\bullet-} \rightarrow ADPA^{\bullet-} + 2Br^- \quad (19)$$

$$2ADPA^{\bullet-} \rightarrow ADPA^{2-} + ADPA^0 \quad (20)$$

Scheme I

$$ADPA^{2-} + Br_2^{\bullet-} \rightarrow ADPA^{\bullet-} + 2Br^- \quad (19)$$

$$ADPA^{\bullet-} + O_2 \rightarrow (ADPA)O_2^{\bullet-} \quad (21)$$

$$(ADPA)O_2^{\bullet-} + ADPA^{2-} \rightarrow (ADPA)O_2^{2-} + ADPA^{\bullet-} \quad (22)$$

$$2ADPA^{\bullet-} \rightarrow ADPA^{2-} + ADPA^0 \quad (20)$$

$$ADPA^{\bullet-} + O_2^{\bullet-} \rightarrow (ADPA)O_2^{2-} \quad (23)$$

$$2(ADPA)O_2^{\bullet-} \rightarrow (ADPA)O_2^{2-} + (ADPA)O_2 \quad (24)$$

Concluding Remarks. This study has established that, at most, only a few percent of the electron-transfer process between $Ru(bpy)_3^{3+}$ and $O_2^{\bullet-}$ results in singlet oxygen formation. It is therefore possible to conclude that the quantitative formation of singlet oxygen via the quenching of $^*Ru(bpy)_3^{2+}$ by O_2 must result from a true energy-transfer mechanism. The alternative route,[1,21] i.e. electron transfer to form $Ru(bpy)_3^{3+}|O_2^{\bullet-}$ followed by a rapid reaction between Ru(III) and $O_2^{\bullet-}$ generating Ru(II) and O_2 ($^1\Delta_g$) appears unacceptable.

(21) Lin, C.-T.; Bottcher, W.; Chou, M.; Creutz, C.; Sutin, N. *J. Am. Chem. Soc.* **1976**, *98*, 6536–6544.

As pointed out above, the recombination process 7 is of sufficient exergonicity to leave molecular oxygen in the $^1\Delta_g$ electronic state ($E \simeq 1$ eV) but insufficient to form $Ru(bpy)_3^{2+}$ in its excited state ($E \simeq 2.1$ eV).[2] Liu et al.[22] showed that exergonic electron-transfer reactions between $Ru(bpy)_3^{3+}$ and several Co(I) complexes resulted in preferential population of electronically excited states of the Ru(II) and/or Co(II) products with minimal ground-state production. The relative slowness of the reaction to form ground-state products was attributed to the very high exergonicity of this process, placing it in the inverted region ($-\Delta G^0 > \lambda$, where λ is the reorganization parameter).[22] In our case, there is a relatively large reorganization energy related to the difference in solvation of O_2 and $O_2^{\bullet-}$ and the different bond lengths in the two species.[23] The value of the overall barrier seems likely to be about the same as the value of ΔG^0 for the reaction leading to O_2 ($^3\Sigma_g^-$), i.e. $-\Delta G^0 \simeq \lambda$. According to this assumption, the O_2 ($^3\Sigma_g^-$) forming process would be barrierless (i.e., very fast) whereas the O_2 ($^1\Delta_g$) forming one, having a smaller driving force, is expected to proceed more slowly because it lies in the normal free energy region. Thus, the lack of singlet oxygen formation is not a surprising result.

Acknowledgment. This research was supported in part by Consiglio Nazionale delle Ricerche of Italy, in part by National Institutes of Health (Grant GM 24235), and in part by Ministero of Pubblica Istruzione of Italy (Quota 40%). The Center for Fast Kinetics Research is jointly supported by the Biomedical Research Technology Program of the Division of Research Resources of the NIH (Grant RR 00886) and by the University of Texas at Austin. The technical assistance of G. Gubellini is appreciated. We thank Prof. M. Maestri for making available to us the continuous-photolysis apparatus and for discussion of the results obtained. Q.G.M. thanks the staff of CFKR for making his visit to the Center (Spring 1987) a most rewarding one.

Registry No. MV^{2+}, 1910-42-5; $ADPA^{2-}$, 113273-49-7; $Ru(bpy)_3^{2+}$, 15158-62-0; $Ru(bpy)_3^{3+}$, 18955-01-6; O_2, 7782-44-7; $O_2^{\bullet-}$, 11062-77-4.

(22) Liu, D. K.; Brunschwig, B. S.; Creutz, C.; Sutin, N. *J. Am. Chem. Soc.* **1986**, *108*, 1749-1755.

(23) We are grateful to Dr. D. Meisel for discussions on this point and to Dr. N. Sutin who took the trouble to clear up some misconceptions.

Substituted Complexes of Enterobactin and Synthetic Analogues as Probes of the Ferric-Enterobactin Receptor in *Escherichia coli*†

David J. Ecker, Lawrence D. Loomis, Marion E. Cass, and Kenneth N. Raymond*

Contribution from the Department of Chemistry, University of California, Berkeley, California 94720. *Received May 14, 1987*

Abstract: The structural requirements for recognition of ferric-enterobactin by the ferric-enterobactin receptor in *Escherichia coli* have been examined with model complexes as probes in mediation, and inhibition, of transport. Kinetically inert, air-stable rhodium(III) tris ligand complexes of catechol and 2,3-dihydroxy-*N*,*N*-dimethylbenzamide (DMB) and a rhodium(III) complex of a close structural analogue of enterobactin, 1,3,5-tris[[(2,3-dihydroxybenzoyl)amino]methyl]benzene (MECAM), were used as probes to study the importance of the ligand amide functional group in complex recognition. The Rh(III)-MECAM complex is a competitive inhibitor of ferric-enterobactin transport. The ferric complex of the same ligand is a transport substrate in *E. coli*. The simple tris(catecholate) complex of rhodium(III), $[Rh(cat)_3]^{3-}$, is *not* an inhibitor of ferric-enterobactin uptake, but the tris complex of the catechoylamide (DMB) *is* potent as an inhibitor. These results indicate that although it is the tris(catecholate) portion of the ferric-enterobactin complex that is recognized by the receptor protein, the amide regions of enterobactin, which link the catechol groups to the cyclic backbone, are also required components in recognition. Consistent with these observations, the ferric complex of the enterobactin analogue TRIMCAM (1,3,5-tris[(2,3-dihydroxybenzyl)carbamoyl]benzene, a structural isomer of MECAM in which the positions of the methyene, carbonyl, and NH groups are reversed) is not recognized by the ferric-enterobactin receptor. Replacement of the amide protons of MECAM with methyl groups does not change the iron transport properties of the ligand. The ferric complex of the N-methylated derivative Me_3MECAM (1,3,5-tris[[methyl(2,3-dihydroxybenzoyl)amino]methyl]benzene) is a substrate for iron(III) transport in vivo. A third derivative of MECAM, MECAM-Me (1,3,5-tris[[(2,3-dihydroxy-4-methylbenzoyl)amino]methyl]benzene), was synthesized to probe the sensitivity of the ferric-enterobactin receptor to changes in the ligand structure near the catechol groups. No iron uptake was observed when *E. coli* cells were given $[Fe(MECAM\text{-}Me)]^{3-}$ or the ferric complex of a sulfonated derivative of MECAM, MECAMS (1,3,5-tris[[(2,3-dihydroxy-5-sulfobenzoyl)amino]methyl]benzene). These experiments demonstrate that it is the tris(catechol)iron(III) portion of the ferric-enterobactin complex that is recognized by the protein receptor, not the enterobactin triserine ring. Furthermore, the carbonyl group is essential for recognition; however, the proton on the amide nitrogen is not. In addition, we have observed that any substitution on the catechol rings opposite the region of attachment to the enterobactin triserine ring (or similar model structure) blocks recognition. Labile trivalent metal ion complexes of enterobactin, as analogues of Fe(III), were prepared to study the effect of the physical properties of the metal ions on the recognition process. These complexes of enterobactin ranged from relatively effective inhibitors of ferric-enterobactin uptake to ineffective inhibitors in the series (with the Fe(III) complex as the reference) Fe > Sc > In ≫ Al > Ga.

Enterobactin is a low molecular weight iron chelating agent (siderophore) produced and excreted by *Escherichia coli* and other enteric bacteria to bind and assimilate extracellular iron.[2,3] After iron complexation, the extracellular ferric-enterobactin complex interacts with a specific receptor in the outer cell membrane, and the complex is taken into the cell by active transport. It has been shown that the ferric complexes of some synthetic analogues of

† Part 39. Coordination Chemistry of Microbial Iron Transport. See ref 6 for the previous paper.

(1) Matzanke, B.; Ecker, D. J.; Yang, T. S.; Huynh, B. H.; Müller, G.; Raymond, K. N. *J. Bacteriol.* **1986**, *167*, 674.

(2) Neilands, J. B. *Annu. Rev. Microbiol.* **1982**, *36*, 285.

(3) Raymond, K. N.; Müller, G.; Matzanke, B. F. *Topics in Current Chemistry*; Boschke, F. L., Ed.; Springer: Berlin, 1984; Vol. 123, pp 50-102.

0002-7863/88/1510-2457$01.50/0